Structure and Disorder in Amorphous Alumina Thin Films: Insights from High-Resolution Solid-State NMR

ARTICLE *in* THE JOURNAL OF PHYSICAL CHEMISTRY C · JULY 2010

Impact Factor: 4.77 · DOI: 10.1021/jp105306r

Structure and Disorder in Amorphous Alumina Thin Films: Insights from High-Resolution Solid-State NMR

Sung Keun Lee,*,† Sun Young Park,† Yoo Soo Yi,† and Jaehyun Moon‡

Laboratory of Physics and Chemistry of Earth Materials, School of Earth and Environmental Sciences, Seoul National University, Seoul 151-742, Korea, and Convergence Components and Materials Research Lab, Electronics and Telecommunications Research Institute, Daejeon 305-350, Korea

Received: June 9, 2010; Revised Manuscript Received: July 15, 2010

Revealing the extent of disorder in amorphous oxides is one of the remaining puzzles in physical chemistry, glass sciences, and geochemistry. Here, we report the ^{27}Al NMR results for amorphous Al_2O_3 thin films obtained from two different deposition methods (i.e., physical vapor-deposition and atomic layer-deposition), revealing two distinct amorphous states defined by a fraction of five-coordinated Al ($^{[5]}$Al). The fractions of $^{[4]}$Al and $^{[5]}$Al are dominant (∼92−95%) in both films. While the overall similarity between these two states suggests a narrow stability of available amorphous states, the fraction of $^{[5]}$Al in atomic layer-deposited thin films is apparently larger and thus more disordered than that in physical vapor-deposited films. Such results require that varying extents of disorder exist in the amorphous oxides prepared under different processing conditions. As the $^{[5]}$Al site (<1%) in crystalline Al_2O_3 is known to control its catalytic ability over $^{[4]}$Al and $^{[6]}$Al, the significant fractions (∼40%) of $^{[5]}$Al in our amorphous thin films suggest that amorphous Al_2O_3 may be potentially useful as a new class of catalysts.

Introduction

Al_2O_3, one of the prototypical covalent oxides along with SiO_2 and B_2O_3, has diverse applications, including in gate microelectronic devices with high dielectric constants and supports for catalytic nanoparticles due to its large band gap and thermal and chemical stability (e.g., see refs 1–3 and references therein). The structure of crystalline Al_2O_3, particularly the Al coordination environment, is known to control its catalytic ability. A minor fraction (<1%) of unsaturated five-coordinated Al ($^{[5]}$Al) sites in γ-alumina shows much stronger affinity to Pt than $^{[4]}$Al and $^{[6]}$Al exhibit.[3] The $^{[6]}$Al/$^{[4]}$Al ratio in an alumina support can affect its catalytic activity in the reduction of NO_x from lean-burn engines.[4] Although the Al coordination environments of crystalline bulk and thin film alumina are relatively well understood,[1,2,5–9] unlike other archetypal glass formers (e.g., see refs 10–17 and reference therein), understanding of the atomic arrangements in amorphous alumina remains illusive due to difficulties in its synthesis through traditional melt-quenching[18] and the lack of suitable experimental probes. Amorphous states of conventional glass formers as well as oxides lacking a glass-forming ability, such as Al_2O_3, however, can be formed via thin film deposition (e.g., see refs 9, 19–22). Recent breakthroughs in two-dimensional (2D) NMR techniques[23–26] allow us to probe the detailed atomic configurations in amorphous thin films.[27]

Indeed, this progress sheds light on a new opportunity to unveil the nature of amorphous solids, one of the fundamental puzzles in modern chemical and physical sciences, by studying diverse oxide thin films produced under varying processing conditions. Whereas the degree of disorder in the oxide thin films, prepared by varying deposition processes, may be different, a formal microscopic model of distinct amorphous states achieved without glass transition in general has not been established.[28] This is in stark contrast to the glass-forming liquids in which their glass transition temperatures (T_g) can be utilized to describe the varying extent of disorder in the oxide glasses.[28] A variable for amorphous solids, analogous to T_g, would thus be necessary to universally describe the varying amorphous states in amorphous solids.

Among the diverse deposition methods, the physical vapor deposition (PVD) from plasma of free radicals from target oxides[9] and the atomic layer deposition (ALD) based on a series of chemical reactions may provide two extreme cases of oxide thin film deposition.[22] As for the latter, the reactivity between the adsorbed precursor molecules and reactant gas can be improved by plasma-enhanced (PE) ALD at a deposition temperature lower than 200 °C, thus enabling applications in organic light-emitting diodes and organic thin film transistor devices (e.g., see refs 29–31). The previous cross-section TEM studies reported that the Al_2O_3 ALD and PVD thin films were amorphous.[21,27] While the amorphous nature of the Al_2O_3 ALD and PVD thin film was confirmed,[21,27] unlike PVD thin films with a significant fraction of $^{[5]}$Al, the amorphous ALD Al_2O_3 film was reported to consist of only $^{[6]}$Al and $^{[4]}$Al (ref 21). Considering the two distinct deposition methods, the difference in coordination environments between ALD and PVD thin films, if it exists, implies that these two thin films may have distinct amorphous structures. Herein, we explore the extent of disorder in amorphous Al_2O_3 thin films using high-resolution solid-state NMR, revealing their amorphous structures. The probed structural variability in amorphous oxide thin films is in turn utilized to propose a process variable with a potential utility to characterize the distinct amorphous states in diverse oxide thin films.

* Corresponding author. Phone: (822) 880-6729. Fax: (822) 871-3269. E-mail: sungklee@snu.ac.kr.
† Seoul National University.
‡ Electronics and Telecommunications Research Institute.

10.1021/jp105306r
Published on Web 07/28/2010

Experimental Section

Thin Film Deposition. Approximately 500 nm-thick Al_2O_3 thin films were deposited on p-type Si(100) substrates by PEALD using trimethylaluminum (TMA) as the aluminum precursor and O_2 mixed with a small amount of N_2 as the oxygen precursor at 473 K with an rf plasma power of 300 W without an external bias. Ar was used as a carrier gas at a pressure of 3.0 Torr.[30] While detailed synthesis conditions for the physical vapor deposition were given in our previous study,[27] ~1.4 μm-thick Al_2O_3 thin film was deposited on a Si_3N_4/Si(100) wafer by rf magnetron sputtering at 5×10^{-6} Torr. PVD was carried out using an Al_2O_3 target of 99.995% purity at an rf power of 500 W at 298 K in Ar as supporting gas. The substrates were chemically etched (PVD film) and mechanically grinded (ALD film) to maximize the NMR signal from the Al_2O_3 thin film. The final thickness of each substrate is ~30 μm (ALD) and ~100 μm (PVD), respectively. Whereas a previous Auger electron spectroscopy study also showed that the composition of the PEALD Al_2O_3 thin film was similar to that of ideal Al_2O_3 (ref 32), the composition of both the amorphous PEALD and PVD thin film was investigated using Al-2p and O-1s XPS, where etched surfaces (approximately 30−60 nm below) were analyzed to minimize the perturbation by carbon contamination. The results show that the composition of the ALD thin film was similar to that of ideal Al_2O_3 and the amorphous PVD Al_2O_3 thin film.

NMR Spectroscopy. ^{27}Al NMR spectra were collected on a Varian 400 solid-state spectrometer (9.4 T) at a Larmor frequency of 104.23 MHz with a 3.2 mm zirconia rotor in a Varian double-resonance probe. A relaxation delay of 1 s and an rf pulse length of 0.3 μs were used to collect the 1D ^{27}Al MAS spectrum. The 2D ^{27}Al triple quantum (3Q) MAS NMR spectra of the amorphous ALD and PVD thin film were collected using a fast-amplitude modulation (FAM)-based shifted-echo pulse sequence[33,34] (1 s relaxation delay−3.0 μs pulse for 3Q excitation−t_1 delay−FAM pulse train with a 0.6 μs pulse−echo delay−a 15 μs soft pulse for echo reconversion−t_2 acquisition) with a spinning speed of 17 kHz (referenced to a 0.1 M $AlCl_3$ solution). While the NMR spectrum for the PVD film was reported,[27] it is also recollected in the current study under identical experimental conditions to the ALD film to check the effect of the processing conditions (PVD vs ALD) on the Al coordination environments in the thin films. The adjustment of rf field strength of each pulse improved the signal/noise ratio in the current experimental data as compared to our previous 2D spectrum for PVD thin film where the rotor background was also not subtracted.[27] To achieve the current signal-to-noise ratio in the 2D spectra, 14 days of collection time for signal averaging of a thin film sample was required. Because there were also signals due to the background $^{[6]}$Al from the empty rotors + Si substrate, the final spectrum was obtained after subtraction of the 2D NMR of the background signals (collected for ~21 days).

Results and Discussion

^{27}Al NMR Results. The features relevant to $^{[4]}$Al (~60 ppm), $^{[5]}$Al (~30 ppm), and $^{[6]}$Al (~0 ppm) (e.g., see refs 35, 36) are revealed in the 1D ^{27}Al MAS NMR spectra of the amorphous PEALD Al_2O_3 thin film (ALD, Figure 1) and are not consistent with the NMR patterns for crystalline alumina polymorphs (e.g., see refs 37–40). This indicates the amorphous nature of the films as also suggested by the previous studies.[21,27] The spectrum of the ALD thin film is similar to that of the amorphous PVD thin film.[27] The feature at ~0 ppm in the PVD thin film is slightly larger than that in the ALD film, indicating a possible difference in structure between these two films. The schematic description of atomic structure of each Al coordination state is also shown.

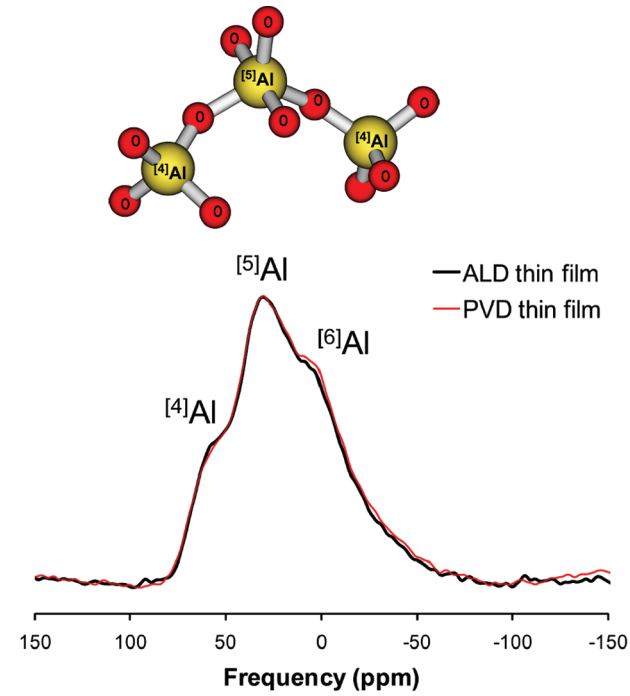

Figure 1. One-dimensional ^{27}Al MAS NMR spectra of an amorphous Al_2O_3 thin film. The black and red spectra refer to spectral features for atomic layer-deposited (ALD, black) and physical vapor Al_2O_3 thin film (PVD, red), respectively. The rotor backgrounds were subtracted from the spectra. The schematic structure of model amorphous Al_2O_3 cluster with $^{[4,5]}$Al is also shown.

Whereas the overlaps among $^{[n]}$Al features due to quadrupolar broadening in the 1D spectra obscure potentially useful structural information, with significantly improved resolution over the 1D MAS NMR (refs 23, 25, 41), the 2D ^{27}Al triple quantum (3Q) MAS NMR spectrum of the amorphous ALD Al_2O_3 thin film shows well-resolved Al coordination environments ($^{[4]}$Al, $^{[5]}$Al, and $^{[6]}$Al) (Figure 2, top). This yields direct and unambiguous experimental evidence for the formation of a significant fraction of $^{[5]}$Al and detailed coordination environments in the amorphous ALD thin film. The Al rotor background consisting mostly of $^{[6]}$Al and a minor fraction of $^{[5]}$Al (Figure 2, bottom right) was observed in the 2D NMR spectrum and was subtracted from the spectra (Figure 2, bottom-left and middle). While the presence of significant fractions of $^{[5]}$Al in the ALD thin film is not consistent with the previous study of similar thin films using electron energy loss spectroscopy (EELS) (ref 21), the EELS analysis based on crystalline oxides consisting only of $^{[4]}$Al and $^{[6]}$Al is not usually suitable to probe the presence of $^{[5]}$Al.

The amorphous ALD and PVD films exhibit similar peak positions and shapes for these Al species. This indicates that the quadrupolar coupling product (P_q) of each $^{[n]}$Al for these two thin films, a measure of Al site distortion,[41] is likely to be identical. Note that the P_q decreases with an increase in Al coordination number from 7.1 ± 0.4 MHz for $^{[4]}$Al, 6.2 ± 0.4 MHz for $^{[5]}$Al, to 4.5 ± 0.4 MHz for $^{[6]}$Al. The similarity in topological disorder (bond angle and length distributions) in these two films is intriguing, particularly considering two distinct processing conditions of thin film depositions (see below for further discussion). While the P_q of Al sites can be affected by the degree of hydration (e.g., see ref 42), the Al−OH group is

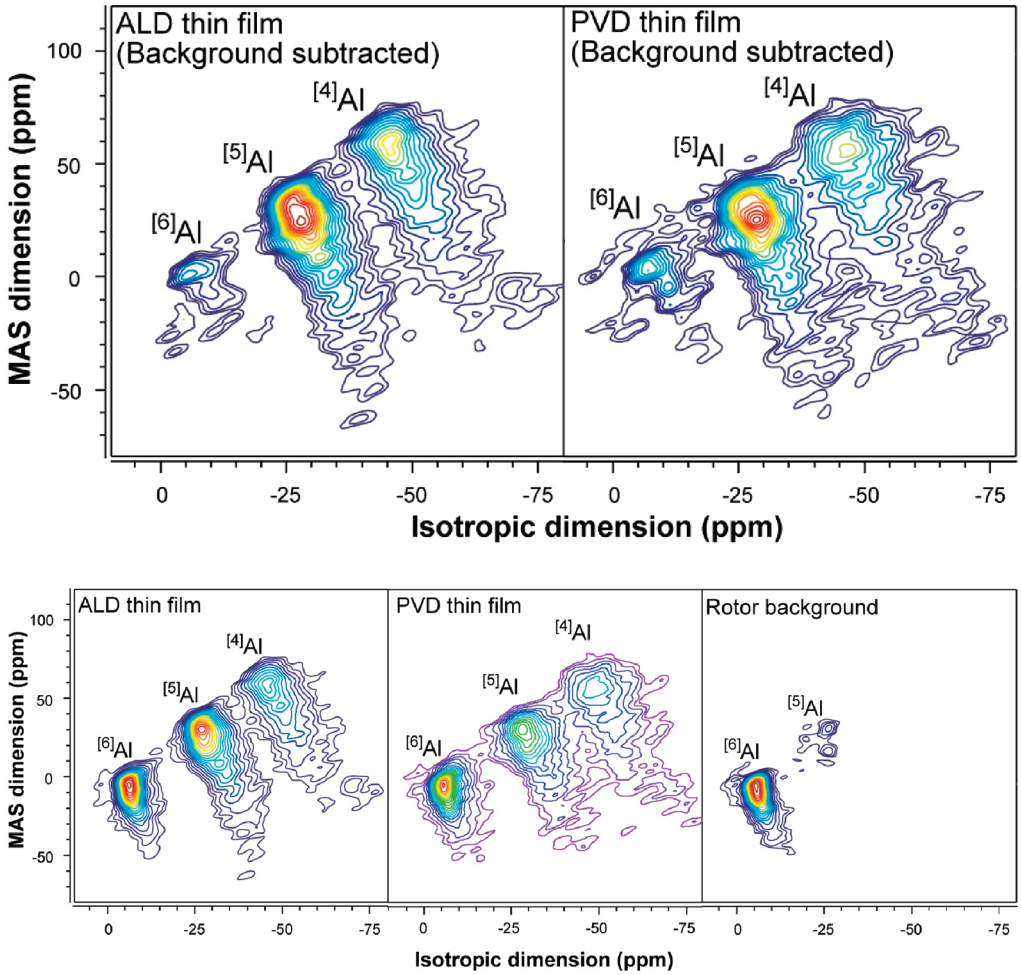

Figure 2. Two-dimensional ^{27}Al 3QMAS NMR spectra of the rotor background subtracted amorphous ALD and PVD thin films. (Top) Contour lines are drawn at 5% intervals from relative intensities of 13−98%, with added lines at 6% and 9%. (Bottom) ^{27}Al 3QMAS NMR spectra of the amorphous ALD Al_2O_3 thin film before background subtraction (left) and NMR rotor background (right). ~14 days of signal averaging was required to achieve the current signal-to-noise ratio of the 2D spectrum for each thin film. Rotor backgrounds (collected for 21 days to achieve a high-quality background spectrum) were subtracted from the original spectra.

not likely to be significant and thus does not add meaningful contribution to the overall Al-27 NMR spectrum of the thin films.[27]

In contrast to the pronounced similarity in topology, the isotropic projection of the spectra for these two amorphous Al_2O_3 thin films unveils the clear differences in the relative fractions of Al species (Figure 3, top). The spectrum of the amorphous ALD Al_2O_3 thin film (black curve) differs from that of the PVD thin film (red curve) in that the $^{[5]}$Al signal is noticeably larger in the ALD thin film. Figure 3 (middle) also shows the results of a simulation with several Gaussian peaks of the total isotropic projection of the ^{27}Al 3QMAS NMR spectra (Figure 3, bottom-left). The NMR signal intensity in the 3QMAS NMR experiment is determined by efficiencies in triple quantum excitation and single quantum reconversion that are mostly dependent on the magnitude of the interactions between the nuclear quadrupolar moment and the electric field gradient (i.e., P_q). The observed NMR signal intensity was, therefore, scaled to take into consideration the magnitude of the quadrupolar interactions characteristic of each Al coordination environment by numerical simulations.[41,43] This method has been successfully used to yield a quantitative fraction of Al coordination environments and structural sites in aluminosilicate glasses at ambient and high pressure.[27,44−47] The calculated 3QMAS efficiency with quadrupolar coupling constant (C_q) at quadrupolar asymmetry parameter (η) of 0.5 is also shown in Figure 3 (bottom-right):[41,43] the calibration factors obtained are 7.9 for $^{[4]}$Al, 9.3 for $^{[5]}$Al, and 10.8 for $^{[6]}$Al, respectively. The fractions obtained from 2D and 1D isotropic projections were divided by the calibration factor for each site, yielding the final fraction of each peak. The calibrated fractions for $^{[4]}$Al, $^{[5]}$Al, and $^{[6]}$Al in the ALD thin film are 54.3%, 40.6%, and 5.1%, whereas those in the PVD thin films are 56.4%, 36.2%, and 7.4%, respectively. Although we note that there could be uncertainty in the absolute fraction of each Al site (e.g., 40.6% vs 36.2% of $^{[5]}$Al in the ALD and PVD thin films, respectively), regardless of the uncertainty, the relative difference in mole fraction $^{[5]}$Al between the amorphous PVD and ALD films (~4−5%) is invariant. The spectra also show a larger $^{[6]}$Al fraction in the PVD thin film. These results thus demonstrate that the detailed amorphous states of these two films are different.

The Extent of Disorder in Alumina Thin Films and Their New Potential Applications. Whereas the difference in the fractions of Al coordination environments between the ALD and PVD thin films could stem from the difference in the deposition conditions, the deposition temperature for each deposition is rather low (below 200 °C), and our XPS study showed that both ALD and PVD thin films have identical O/Al ratios, similar to ideal Al_2O_3. The effects of temperature and composition are thus likely to be insignificant. The PVD alumina

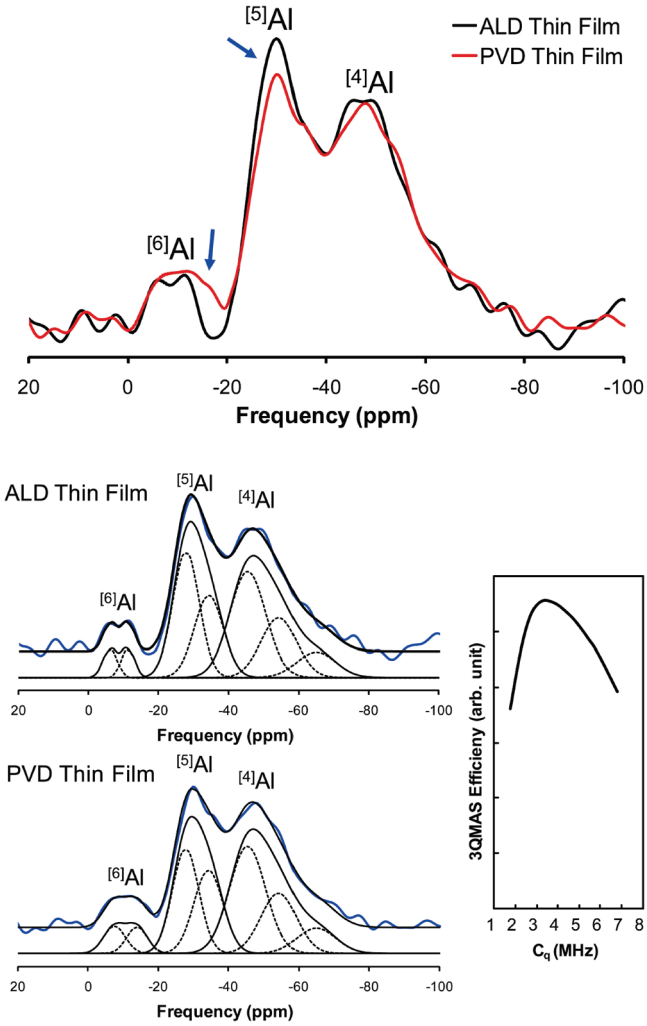

Figure 3. (Top) Total isotropic projections (total sum of the data parallel to MAS dimension) of the ^{27}Al 3QMAS NMR spectra for the Al_2O_3 thin films are shown as labeled. (Bottom-left) Results of simulating Gaussian functions (thin black lines) of the isotropic projection of the ^{27}Al 3QMAS NMR spectra for the amorphous ALD Al_2O_3 thin film and PVD thin film. The thick blue lines refer to the experimental spectra. Note that identical simulation parameters (width, peak positions) are used for all of the Gaussian functions for Al coordination environments in both films. (Bottom-right) Calculated dependence of triple-quantum magic-angle spinning (3QMAS) efficiency (excitation of triple quantum coherence and reconversion into single quantum coherence) on C_q using the Simpson[43] for spin 5/2 nuclei with η of 0.5, the rf field strength of ~120 kHz, and pulse sequences used for the current experiment.

thin film (~1.4 μm) was much thicker than the ALD thin film (~500 nm), which could have contributed to the difference in amorphous states manifested in the coordination environments. Because the thickness effect is likely due to the effect of surface layers close to the substrate and surface,[1,21] considering the relatively thick nature of the current thin films, the surface/substrate effect only partly contributes to the changes in overall coordination environment. The result thus indicates that this is mostly due to an intrinsic difference in amorphous states caused by the fundamental difference in thin film processing (PVD vs ALD), as was also expected from the difference in their macroscopic properties.[29–31]

Glasses and amorphous solids are two fundamental classes of noncrystalline solids. The variability of structure in the glasses can be tuned by controlling the quench rate and thus the glass transition temperature, below which the structures of supercooled

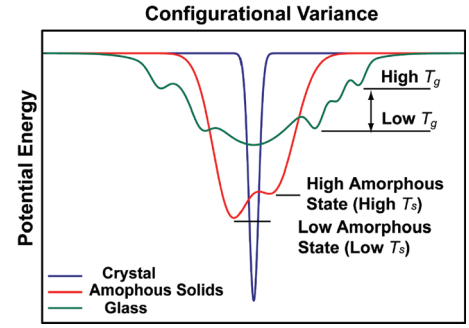

Figure 4. Schematic diagram of energy landscapes (potential energy vs configurational variance) for crystalline materials (blue), glassy materials (red), and amorphous solids (green curve). T_g and T_s denote the glass transition temperature for glass-forming liquids and the fictitious temperature characterizing amorphous solids, respectively.

liquids are frozen. By definition, amorphous solids do not undergo glass transition from melts, and a microscopic variable with universality describing their varying amorphous states has not been available. The above NMR results with varying fractions of Al coordination numbers between two films may be helpful to quantify the extent of disorder in these thin films.

On the basis of the bond valence argument, the energy of the $^{[5]}$Al cluster is expected to be higher than that of the $^{[4]}$Al and $^{[6]}$Al clusters, and the fraction of $^{[5]}$Al [i.e., $X_{\text{Al-5}} = {}^{[5]}\text{Al}/({}^{[4]}\text{Al} + {}^{[5]}\text{Al} + {}^{[6]}\text{Al})$] can thus be regarded as the degree of disorder in the amorphous oxides, which increases with increasing $^{[5]}$Al content. Assuming a constant energy difference, $\Delta\varepsilon$, between $^{[5]}$Al and other Al species based on the two-level system[48] and upon introducing the fictitious temperature (T_s) below which the amorphous states are frozen from the processing of the films, the mole fraction $X_{\text{Al-5}}(T_s)$ of $^{[5]}$Al can now be simply expressed as

$$X_{\text{Al-5}}(T_s) = \frac{1}{\exp[\Delta\varepsilon/kT_s] + 1} \quad (1)$$

where k is the Boltzmann constant. While T_s is fictitious in a way that it describes the amorphous states from the Al coordination environments, it captures the complexity of relaxation of involved species through the deposition process. $X_{\text{Al-5}}$ increases with increasing T_s and decreasing $\Delta\varepsilon$. If $\Delta\varepsilon$ values for both PVD and ALD are identical, the difference in amorphous states between the films can be attributed to the difference in T_s for each process (Figure 4, red curve). T_s for ALD is apparently higher than that for PVD processing based on the larger $^{[5]}$Al fraction. Furthermore, taking into consideration the varying and/or unknown amount of $\Delta\varepsilon$ for diverse deposition processes, $T_s/\Delta\varepsilon$ (i.e., normalized fictitious temperature) can then be effective in characterizing distinct amorphous states: the estimated $T_s/\Delta\varepsilon$ values for the amorphous ALD and PVD thin films are 0.32 and 0.21, respectively. Because T_s increases with increasing degree of disorder, the T_s or $T_s/\Delta\varepsilon$ can be useful for quantifying the degree of disorder in amorphous alumina thin films. We note that as only two extreme cases of thin film depositions are tested here, further extensive studies of Al coordination number in thin films deposited with varying deposition processes, thin film thickness, and temperature would be certainly necessary to yield sufficient justification for the modeling of amorphous states with T_s.

As compared to the crystalline materials characterized with a narrow range of configurational variance in the energy landscape (Figure 4, blue curve), a potentially wide range of

configurational states in the glass can be tuned by controlling the glass transition temperature (i.e., fictive temperature) (Figure 4, green curve). The pronounced similarity between the two amorphous films is intriguing in that the amorphous states produced by two distinct deposition methods are not significantly different. This suggests that there is a rather narrow window of possible amorphous states in Al_2O_3 (Figure 4, red curve). Additionally, a clear difference in amorphous states between the two films shown in Figures 2 and 3 is also surprising, suggesting the existence of varying amorphous states. Therefore, the small difference in these amorphous states (evidenced by varying fractions of Al coordination states) in the amorphous thin film oxides can now be probed and modeled with T_s.

We finally note that, on the basis of the recently revealed catalytic control of $^{[5]}$Al over $^{[4,6]}$Al in crystalline Al_2O_3 (ref 3), the significant fraction (~40%) of $^{[5]}$Al in amorphous PVD and ALD alumina thin films implies potential utility of these films as surface catalysts (and catalytic supports). We suggest that amorphous alumina-based catalysts can thus be effective in the removal of NO_x (ref 4) and in enhancing the catalytic activity at surfaces remarkably due to the $^{[5]}$Al in the amorphous thin films.

In conclusion, we have elucidated the similarity in the overall structure, implying a narrow window of amorphous states in the thin film oxides. The current study also highlights the first experimental evidence of the varying amorphous states and structures obtained from different processing conditions of oxide thin film deposition, revealing amorphous states in archetypal amorphous oxides using high-resolution solid-state NMR. These differences can be accounted for by a concept utilizing the fictitious temperature, a process variable analogous to the glass transition temperature. The concept of the fictitious temperature may be useful to describe the nature of the amorphous states in diverse amorphous oxide thin film without glass transition from melts. The current study also highlights that 2D solid-state NMR techniques can be useful in characterizing diverse amorphous oxide thin films.

Acknowledgment. This work was supported by the Korea Science & Engineering Foundation through the National Research Laboratory Program to S.K.L. (2007-000-20120). We thank S. B. Lee for discussion on thin film deposition and two anonymous reviewers for constructive suggestions and comments.

References and Notes

(1) Kresse, G.; Schmid, M.; Napetschnig, E.; Shishkin, M.; Kohler, L.; Varga, P. *Science* **2005**, *308*, 1440.
(2) Stierle, A.; Renner, F.; Streitel, R.; Dosch, H.; Drube, W.; Cowie, B. C. *Science* **2004**, *303*, 1652.
(3) Kwak, J. H.; Hu, J. Z.; Mei, D.; Yi, C. W.; Kim, D. H.; Peden, C. H. F.; Allard, L. F.; Szanyi, J. *Science* **2009**, *325*, 1670.
(4) Thibault-Starzyk, F.; Seguin, E.; Thomas, S.; Daturi, M.; Arnolds, H.; King, D. A. *Science* **2009**, *324*, 1048.
(5) Freysoldt, C.; Rinke, P.; Scheffler, M. *Phys. Rev. Lett.* **2007**, *99*, 086101.
(6) Eng, P. J.; Trainor, T. P.; Brown, G. E.; Waychunas, G. A.; Newville, M.; Sutton, S. R.; Rivers, M. L. *Science* **2000**, *288*, 1029.
(7) Barth, C.; Reichling, M. *Nature* **2001**, *414*, 54.
(8) Levin, I.; Brandon, D. *J. Am. Ceram. Soc.* **1998**, *81*, 1995.
(9) Chou, T. C.; Nieh, T. G. *Thin Solid Films* **1992**, *221*, 89.
(10) Lacks, D. J. *Phys. Rev. Lett.* **2000**, *84*, 4629.
(11) Lee, S. K.; Eng, P. J.; Mao, H. K.; Meng, Y.; Newville, M.; Hu, M. Y.; Shu, J. F. *Nat. Mater.* **2005**, *4*, 851.
(12) Lee, S. K.; Mibe, K.; Fei, Y.; Cody, G. D.; Mysen, B. O. *Phys. Rev. Lett.* **2005**, *94*, 165507.
(13) Youngman, R. E.; Haubrich, S. T.; Zwanziger, J. W.; Janicke, M. T.; Chmelka, B. F. *Science* **1995**, *269*, 1416.
(14) Ferlat, G.; Charpentier, T.; Seitsonen, A. P.; Takada, A.; Lazzeri, M.; Cormier, L.; Calas, G.; Mauri, F. *Phys. Rev. Lett.* **2008**, 101.
(15) Greaves, G. N.; Sen, S. *Adv. Phys.* **2007**, *56*, 1.
(16) Sato, T.; Funamori, N. *Phys. Rev. Lett.* **2008**, *101*, 255502.
(17) Murakami, M.; Bass, J. D. *Phys. Rev. Lett.* **2010**, 104.
(18) Rosenflanz, A.; Frey, M.; Endres, B.; Anderson, T.; Richards, E.; Schardt, C. *Nature* **2004**, *430*, 761.
(19) Swallen, S. F.; Kearns, K. L.; Mapes, M. K.; Kim, Y. S.; McMahon, R. J.; Ediger, M. D.; Wu, T.; Yu, L.; Satija, S. *Science* **2007**, *315*, 353.
(20) Dupree, R.; Farnan, I.; Forty, A. J.; Elmashri, S.; Bottyan, L. *J. Phys. (Paris)* **1985**, *46*, 113.
(21) Kimoto, K.; Matsui, Y.; Nabatame, T.; Yasuda, T.; Mizoguchi, T.; Tanaka, I.; Toriumi, A. *Appl. Phys. Lett.* **2003**, *83*, 4306.
(22) Leskela, M.; Ritala, M. *Thin Solid Films* **2002**, *409*, 138.
(23) Frydman, I.; Harwood, J. S. *J. Am. Chem. Soc.* **1995**, *117*, 5367.
(24) Lee, S. K.; Deschamps, M.; Hiet, J.; Massiot, D.; Park, S. Y. *J. Phys. Chem. B* **2009**, *113*, 5162.
(25) Massiot, D.; Touzo, B.; Trumeau, D.; Coutures, J. P.; Virlet, J.; Florian, P.; Grandinetti, P. J. *Solid State Nucl. Magn. Reson.* **1996**, *6*, 73.
(26) Stebbins, J. F.; Xu, Z. *Nature* **1997**, *390*, 60.
(27) Lee, S. K.; Lee, S. B.; Park, S. Y.; Yi, Y. S.; Ahn, C. W. *Phys. Rev. Lett.* **2009**, *103*, 095501.
(28) Elliot, S. R. *Physics of Amorphous Materials*; John Wiley & Sons: New York, 1988.
(29) Lim, J. W.; Yun, S. J. *Electrochem. Solid-State Lett.* **2004**, *7*, F45.
(30) Yun, S. J.; Lim, J. W.; Lee, J. H. *Electrochem. Solid-State Lett.* **2004**, *7*, C13.
(31) Groner, M. D.; Fabreguette, F. H.; Elam, J. W.; George, S. M. *Chem. Mater.* **2004**, *16*, 639.
(32) Lim, J. W.; Yun, S. J.; Lee, J. H. *Electrochem. Solid-State Lett.* **2005**, *8*, F25.
(33) Madhu, P. K.; Goldbourt, A.; Frydman, L.; Vega, S. *Chem. Phys. Lett.* **1999**, *307*, 41.
(34) Vosegaard, T.; Massiot, D.; Grandinetti, P. J. *Chem. Phys. Lett.* **2000**, *326*, 454.
(35) Stebbins, J. F.; Kroeker, S.; Lee, S. K.; Kiczenski, T. J. *J. Non-Cryst. Solids* **2000**, *275*, 1.
(36) Yarger, J. L.; Smith, K. H.; Nieman, R. A.; Diefenbacher, J.; Wolf, G. H.; Poe, B. T.; McMillan, P. F. *Science* **1995**, *270*, 1964.
(37) Huggins, B. A.; Ellis, P. D. *J. Am. Chem. Soc.* **1992**, *114*, 2098.
(38) Lippmaa, E.; Samoson, A.; Magi, M. *J. Am. Chem. Soc.* **1986**, *108*, 1730.
(39) Wang, J. A.; Bokhimi, X.; Morales, A.; Novaro, O.; Lopez, T.; Gomez, R. *J. Phys. Chem. B* **1999**, *103*, 299.
(40) Kim, H. J.; Lee, H. C.; Lee, J. S. *J. Phys. Chem. C* **2007**, *111*, 1579.
(41) Baltisberger, J. H.; Xu, Z.; Stebbins, J. F.; Wang, S.; Pines, A. *J. Am. Chem. Soc.* **1996**, *118*, 7209.
(42) Kentgens, A. P. M.; Igua, D.; M., K.; Koller, H. *J. Am. Chem. Soc.* **2001**, *123*, 2925.
(43) Bak, M.; Rasmussen, J. T.; Nielsen, N. C. *J. Magn. Reson.* **2000**, *147*, 296.
(44) Lee, S. K. *J. Phys. Chem. B* **2004**, *108*, 5889.
(45) Lee, S. K.; Cody, G. D.; Fei, Y. W.; Mysen, B. O. *J. Phys. Chem. B* **2008**, *112*, 11756.
(46) Lee, S. K.; Stebbins, J. F. *Geochim. Cosmochim. Acta* **2009**, *73*, 1109.
(47) Lee, S. K.; Lee, B. H. *J. Phys. Chem. B* **2006**, *110*, 16408.
(48) Lee, S. K.; Eng, P.; Mao, H. K.; Shu, J. F. *Phys. Rev. B* **2008**, *78*, 214203.

JP105306R